



ORIGINAL ARTICLE

Comparative study of transition metal-doped calcined Malaysian dolomite catalysts for WCO deoxygenation reaction

R.S.R.M. Hafriz^{a,c}, I. Nor Shafizah^a, A. Salmiaton^{a,b,*}, N.A. Arifin^c, R. Yunus^a, Y.H. Taufiq Yap^b, S. Abd Halim^c

^a Department of Chemical and Environmental Engineering, Faculty of Engineering, Universiti Putra Malaysia, 43400 UPM Serdang, Selangor, Malaysia

^b Catalyst Science and Technology Research Center (PutraCat), Universiti Putra Malaysia, 43400 UPM Serdang, Selangor, Malaysia

^c Institute of Sustainable Energy, Universiti Tenaga Nasional, 43000 Kajang, Selangor, Malaysia

Received 5 June 2020; accepted 22 September 2020

Available online 7 October 2020

KEYWORDS

Dolomite;
Deoxygenation;
Green fuel;
Pyrolysis;
Waste Cooking Oil (WCO)

Abstract In the present work, nickel (Ni), zinc (Zn), copper (Cu), cobalt (Co) and iron (Fe) are tested as catalyst dopants on Malaysian dolomite calcined at $T = 900\text{ }^{\circ}\text{C}$ (CMD900). The physicochemical properties of all synthesised catalyst are investigated by X-ray diffraction, Brunauer–Emmett–Teller surface area, temperature-programmed desorption of carbon dioxide and scanning emission microscopy. The synthesised catalysts are tested on the basis of the deoxygenation (DO) reaction of waste cooking oil to produce liquid fuels under N_2 atmosphere. The chemical composition of the liquid product is identified by gas chromatography–mass spectroscopy. The overall study suggests that Ni/CMD900 catalyst exhibits the highest performance with over 67.0% conversion and high selectivity (80.2%) with a high proportion of saturated linear hydrocarbons that corresponds to green diesel. Result indicates that Ni/CMD900 is a highly potential DO catalyst with 19.8% oxygenated compound, which is favourable for decarboxylation and/or decarboxylation predominates.

© 2020 The Authors. Published by Elsevier B.V. on behalf of King Saud University. This is an open access article under the CC BY-NC-ND license (<http://creativecommons.org/licenses/by-nc-nd/4.0/>).

* Corresponding author at: Department of Chemical and Environmental Engineering, Faculty of Engineering, Universiti Putra Malaysia, 43400 UPM Serdang, Selangor, Malaysia.

E-mail address: mie@upm.edu.my (A. Salmiaton).

Peer review under responsibility of King Saud University.



Production and hosting by Elsevier

1. Introduction

The increasing growth and modernisation of the economy intensify the demand for transportation fuel and power consumption rapidly in the last few decades (Seifi and Sadrameli, 2016). Dependence on fossil energy as the ultimate energy source has resulted in the exhaustion of the world's petroleum reserves and has led to energy price crisis (Charusiri

and Vitidsant, 2017; Fazril et al., 2020). The shortage and price hike of fossil fuels accompanied by vast CO₂ emissions have triggered a worldwide search for alternative and sustainable resources (Sousa et al., 2018). A wide consumption of fossil fuel in combustion largely contributes to the increase in greenhouse gas emissions in the atmosphere, thereby resulting in global climate change, acid rain and ozone layer depletion (Wang et al., 2017). Thus, the reduction of anthropogenic CO₂ emissions is important to mitigate global warming (Arstad et al., 2014). These environmental issues have inspired researchers to find an alternative green fuel from renewable resources (Asikin-Mijan et al., 2018). Green fuel consists of free-oxygenated hydrocarbon compound, which is also known as clean-burning fuel with significantly low sulphur and aromatics contents and high cetane number, lubricity and renewability (Alsultan et al., 2017). Green fuel is carbon neutral because the CO₂ released by its combustions is neutralised by the CO₂ utilisation for plant growth, which can be used back as a raw material for biofuel generation; as a result, the net CO₂ level in the atmosphere is unaffected (Pattanaik and Misra, 2017).

Extensive research on biofuel generation from many renewable feedstocks, such as edible biomass and triglyceride-based biomass, has gained momentum in recent years. Triglyceride-based sources have a molecular network similar to hydrocarbon, which plays a substantial role in biofuel production (Seifi and Sadrameli, 2016). WCO can be a promising feedstock for biofuel production because the main composition in waste cooking oil (WCO) is triglyceride, and the fatty acid fractions are derived from cooking oil such as sunflower, palm, soybean, and coconut (Wang et al., 2017). These sources are considered economically viable because of their low cost and high availability, and their valorisation can also solve the issues associated with their disposal. The disposal of WCO is important in terms of the economy, environment protection and personnel safety. The abundance of WCO produced annually throughout the world has increased the demand for its rational disposal and reutilisation (Chen et al., 2014). The lack of a proper disposal collection system can result in significant disposal, odour and pollution problems (Chang et al., 2017). In the United States, 10 million tons of WCO are produced each year, whilst China generates 5 million tons of WCO annually (Lam et al., 2016). The WCO collected from restaurants, hotels, university cafeterias, hospitals, and refectories are disposed to landfills, evacuated to sewers, and utilised in the soap industry (Trabelsi et al., 2018). The use of WCO as the second generation biofuel feedstock not only improves the quality of the environment but also solves the waste disposal problem (Romero et al., 2016; Hafriz et al., 2018). Furthermore, the cost of raw material is a dominant part of the overall cost of green fuel production. Thus, the use of non-expensive, sustainable and non-value-added WCO could improve the overall financial viability (Wako et al., 2018) and promote a circular economy. However, the direct use of WCO as fuel in a diesel engine can cause problems and air pollution because of particulate matter deposits (Trabelsi et al., 2018). Therefore, several pre-treatment processes, including pre-heating, mixing with gas oil with low viscosities, emulsification, pyrolysis and transesterification, have been used to improve the properties of these edible oils (Trabelsi et al., 2018). Amongst the pre-treatment methods, pyrolysis deoxygenation (DO) is considered an inexpensive and effective way to convert WCO into

lighter fractions of gasoline boiling range (Wako et al., 2018). Pyrolysis DO is a thermochemical method that breaks the chemical bonds of materials and converts them into a potential fuel product in three phases, which are liquid product, carbon-rich solid residues, and gaseous product, under oxygen-absence circumstances at a rapid heating rate (Chen et al., 2014; Lam et al., 2016; Dong and Zhao, 2018). Pyrolysis product is predominantly composed by alkanes, alkenes, dienes, aromatic compound, carboxylic acids with carbon ranging from 4 to 20 and other unsaturated compounds (Trabelsi et al., 2018). In addition to pyrolysis DO, hydrodeoxygenation (HDO) technologies have been used extensively to produce hydrocarbon-based fuel (Asikin-Mijan et al., 2016). HDO is a cracking process under high pressure in a H₂ gas environment, which produces water as a by-product (Asikin-Mijan et al., 2018). However, it requires a high amount of H₂ gases and high reaction pressure. Hence, due to the considerable consumption of H₂, complicated equipment and high reaction operating conditions in HDO process, DO reaction is preferred because it is more economical, effective, more flexible in the choice of raw materials and suitable for industrial practices (Wang et al., 2017; Alsultan et al., 2017).

The pyrolysis DO of edible oils using a selected heterogeneous catalyst is a potential candidate for renewable process-based industrialisation instead of a homogeneous catalyst. The heterogeneous catalyst is easily recycled and regenerated and is environmentally friendly, thereby increasing the product yield and decreasing the cost of liquid fuels (Wako et al., 2018). In recent years, as an environmentally friendly and low-cost value-added industrial mineral, dolomite is mainly used in construction and agricultural fields as a fertilizer. Recently, dolomites have attracted much attention as a promising basic solid catalyst for biofuel production (Mao et al., 2017; Shahrzuzaman et al., 2018). Dolomites, CaMg(CO₃)₂, which consist of calcium carbonate (CaCO₃), magnesium carbonate (MgCO₃) and a very small percentage of other compounds, is widely found in sedimentary rocks deposited in marine and continental lacustrine settings (Shajaratun Nur et al., 2014). Based on recent studies by Mohammed et al. (2013) and Zhou et al. (2017) with focus on the calcination behaviour of dolomite, dolomite with high calcite content requires temperature above 900 °C for calcination, which contributes to the excellent performance in catalytic reactions.

Low-cost transition metal oxides (TMOs) (e.g., Ni, Co, W, Mo, Cu, Fe and Zn) that has been extensively investigated as alternative to expensive noble metals (e.g., Pt and Pd) proven to successfully enhance the catalytic activity in DO process thus increase the yield of hydrocarbon fractions (Alsultan et al., 2017). Asikin-Mijan et al. (2018) reported that Ni-based catalyst was proven to be a good potential catalyst in improving the yield of pyrolysis oil via DO reaction. However, the presence of high acidity sites resulted in extensive deactivation due to catalyst coking and tar formation. Meanwhile, Co-based catalyst respond differently because its acidity was lower than that of Ni catalyst. Nevertheless, this paper (Asikin-Mijan et al., 2018) also reported the synergy effect of the acidity and basicity of Ca/CaO catalyst and improved the quality of green fuel and reduction in coke formation during DO reaction. The conjugation of basic and acid metals is needed to become highly selective towards the high formation of light hydrocarbon fractions (Alsultan et al., 2017). To the best

knowledge of the author, no other report has covered in-depth studies of using a low-cost Malaysian dolomite via catalytic pyrolysis of WCO, to date. The present study aims to synthesise Malaysian dolomite-based catalyst, which has a basic characteristic and has been doped using selected transition metals, such as nickel (Ni), zinc (Zn), copper (Cu), cobalt (Co), and iron (Fe), which has an acidic characteristic. The physicochemical properties of the synthesised catalyst were examined. The present work also investigates the activity of the synthesised catalysts in the DO reaction of WCO. The yield and the characteristic of the liquid products were also evaluated in this study.

2. Experimental

2.1. Material

Analytical grade nitrate salts of various metals, including iron (III) nitrate nanohydrate, $(\text{Fe}(\text{NO}_3)_3 \cdot 9\text{H}_2\text{O})$ (99.95%), Cobalt (II) nitrate hexahydrate $(\text{Co}(\text{NO}_3)_2 \cdot 6\text{H}_2\text{O})$ (99.95%), nickel (II) nitrate hexahydrate, $(\text{Ni}(\text{NO}_3)_2 \cdot 6\text{H}_2\text{O})$ (99.95%), Copper (II) nitrate trihydrate $(\text{Cu}(\text{NO}_3)_2 \cdot 3\text{H}_2\text{O})$ (99.95%) and zinc nitrate hexahydrate $(\text{Zn}(\text{NO}_3)_2 \cdot 6\text{H}_2\text{O})$ (99.95%) were purchased from System Chemicals Sdn. Bhd. Grinded Malaysian dolomite ($\text{CaMg}(\text{CO}_3)_2$) was obtained from Northern Dolomite Sdn. Bhd. (Perlis, Malaysia). The grinded Malaysian dolomite was calcined at 900 °C for 4 h and was denoted as CMD900. Malaysian dolomite contained 31.0% of CaO and 20.0% of MgO. The WCO was collected from residential area in Selangor, Malaysia and treated by centrifugation at 6000 rpm for 30 min to remove the sediments from the WCO. Subsequently, the treated WCO was filtered using a wire sieve strainer (250 μ mesh size) to decant the food residue. The composition of the WCO used was analysed using GC-MS analysis with 1.97% hydrocarbon and 98.02% oxygenated compound. The composition of carboxylic acid in WCO is presented in Table 1. Industrial-grade nitrogen gas, N_2 , (99.95%) was supplied by Smart Biogas Sdn. Bhd. GC analytical-grade n-Hexane (>98%) was acquired from Merck.

2.2. Catalyst preparation by precipitation technique

The 5 wt% of x/CMD900 catalyst was prepared by using simple liquid-liquid blending (precipitation technique) with 5 wt

% loading of a transition metal x = Fe, Co, Ni, Cu and Zn onto CMD900. A known amount of metal nitrate was dissolved in deionised water. A total of 14 g of CMD900 was dispersed into 100 ml of deionised water under vigorous stirring at 60 °C. Subsequently, the aqueous solution of a metal nitrate was added dropwise into the slurry of CMD900 with agitation for 4 h. The mixture was stirred vigorously (with 400 rpm) and heated at 60 °C for 4 h. The sample was recovered by filtration and rinsed several times with deionised water. The sample was dried at 120 °C overnight. Subsequently, the dried sample was grinded and sieved using a mesh with a size of 250 μm . Finally, the sample was calcined at 900 °C for 4 h under a continuous flow of N_2 gas. The aforementioned procedure was repeated using $\text{Fe}(\text{NO}_3)_3 \cdot 9\text{H}_2\text{O}$, $\text{Co}(\text{NO}_3)_2 \cdot 6\text{H}_2\text{O}$, $\text{Ni}(\text{NO}_3)_2 \cdot 6\text{H}_2\text{O}$, $\text{Cu}(\text{NO}_3)_2 \cdot 3\text{H}_2\text{O}$ and $\text{Zn}(\text{NO}_3)_2 \cdot 6\text{H}_2\text{O}$ and will be denoted as Fe/CDM900, Co/CDM900, Ni/CDM900, Cu/CDM900 and Zn/CDM900, respectively.

2.3. Catalyst characterisation

The XRD analysis was performed to identify the phase and chemical composition of the synthesised catalysts using Shimadzu XRD-600 with scan ranges from $2\theta = 20-80^\circ$ and scanning rate at $2^\circ/\text{min}$. Cu K α radiation source was generated at 40 kV and 40 mA with a broad focus of 2 kW and 7 kW, respectively. The XRD patterns were compared in accordance with the Joint Committee on Powder Diffraction Standard (JCPDS) file. The surface area and porosity of the synthesised catalysts were determined by the Brunauer-Emmett-Teller (BET) method using a quantachrome instrument (model Autosorb-1). The sample was degassed at 150 °C overnight and was flown with N_2 gas in a vacuum chamber at -196°C for the desorption and adsorption processes. The basicity of the synthesised catalysts was investigated using temperature-programmed desorption (TPD) with CO_2 as probe molecules. The TPD- CO_2 was performed using a Thermo Finnigan TPD/R/O 1100 instrument equipped with a thermal conductivity detector (TCD). The samples were pretreated with N_2 gas flow at 30 min at 250 °C. Subsequently, the samples were exposed to CO_2 for 1 h to allow the adsorption process. The desorption of CO_2 was detected by TCD under helium gas flow from 50 °C to 900 °C for 30 min. The surface morphology of the synthesised catalysts was examined by scanning emission microscopy (SEM) using JEOL SEM (JSM-6400). The sample was

Table 1 Composition of carboxylic acid in WCO after pretreatment.

Carboxylic acid	Systematic name	Formula	Structure	Total area %
<i>Saturated</i>				
Caproic acid	Hexanoic	$\text{C}_6\text{H}_{12}\text{O}_2$	C6:0	1.84
Caprylic acid	Octanoic	$\text{C}_8\text{H}_{16}\text{O}_2$	C8:0	0.40
Lauric acid	Dodecanoic	$\text{C}_{12}\text{H}_{24}\text{O}_2$	C12:0	0.64
Myristic acid	Tetradecanoic	$\text{C}_{14}\text{H}_{28}\text{O}_2$	C14:0	2.78
Palmitic acid	Hexadecanoic	$\text{C}_{16}\text{H}_{32}\text{O}_2$	C16:0	53.24
Stearic acid	Octadecanoic	$\text{C}_{18}\text{H}_{36}\text{O}_2$	C18:0	2.13
<i>Unsaturated</i>				
Oleic acid	<i>cis</i> -9-Octadecanoic	$\text{C}_{18}\text{H}_{34}\text{O}_2$	C18:1	32.52
Others	–	–	–	6.45

dispersed on the stub coated with a thin layer of gold by using BIO-RAS sputter.

2.4. Pyrolysis DO reaction of WCO

The DO reactions were conducted in a fractionated cracking system with two condensers as depicted in Fig. 1. In a typical experiment, 150.0 g of WCO and 7.5 g of catalyst amount were added to the reactor. The reaction was performed under inert N₂ flow at a flow rate of 150 cm³/min. The DO reaction was performed at a reaction temperature of 390 °C ± 5 °C for 30 min. The vapour generated during the DO reaction flowed through a Graham condenser (250–270 °C) and condensed into a liquid product in a water-cooling condenser (25 °C). The liquid product and residual oil-coke were collected from the collecting and reaction flasks, respectively. The gas product was released through the gas outlet without conducting further analysis. Two liquid fractions and a small amount of soap were observed in aqueous (top layer) and organic phases (bottom layer) of the collecting flask. These phases were then separated by decantation. The soap was removed by filtration using a filter paper while the pyrolysis oil was analysed with GC-MS. The yield of the pyrolysis oil and the conversion of WCO was calculated by using mass balance (Eq. (1) and (2)) (Choi et al., 2018).

$$\text{Yield of oil product (\%)} = \frac{\text{mass of oil product (g)}}{\text{mass of WCO (g)}} \times 100\% \quad (1)$$

$$\text{Conversion of WCO} \left(\begin{array}{l} \text{\%} = \frac{\text{mass of WCO (g)}}{\text{mass of oil WCO (g)}} \\ \text{\%} = \frac{-\text{mass of coke (g)}}{\text{mass of oil WCO (g)}} \end{array} \right) \times 100\% \quad (2)$$

2.5. Product analysis

The composition of pyrolysis oil products was analysed by gas chromatography–mass spectrometry (GC-MS, Shimadzu QP2010) equipped with non-polar ZB-5MS column (30 m × 0.25 mm × 0.25 μm) in a split mode. The identification of unsaturated hydrocarbons was performed by interpreting GC-MS data and by comparing with the National Institute of Standards and Testing (NIST) library. The hydrocarbon fraction (%) was determined by the total area of the chromatogram of saturated (n-alkane) and unsaturated (n-alkene) straight-chain hydrocarbons (C8-C20), as shown in Eq. (3). Meanwhile, product selectivity was determined by Eq. (4) (Dong and Zhao, 2018), and the percentage removal of oxygenated compound was calculated by Eq. (5):

$$\text{Hydrocarbon (\%)} = \frac{\sum \text{Area of alkene (C8 - C20)} + \sum \text{Area of alkane (C8 - C20)}}{\sum \text{Area of total product}} \quad (3)$$

$$\text{Product selectivity (\%)} = \frac{\text{Area of desired product}}{\text{Total area of the product}} \times 100\% \quad (4)$$

$$\begin{aligned} \text{Percentage removal of oxygenated compound (\%)} \\ = \frac{\sum \text{Area of oxygenated compound of WCO} - \sum \text{Area of oxygenated compound of pyrolysis oil}}{\sum \text{Area of oxygenated compound of WCO}} \times 100\% \end{aligned} \quad (5)$$

2.6. Analysis of pyrolysis oil properties

Pyrolysis oil generated using Ni/CMD900 was selected, and its properties were analysed. The analysis behaviour of the biofuel properties has been compared with the other properties of fuel, such as pyrolysis oil from palm oil, diesel fuel, and hydrocarbon biofuel, based on literatures. The property analysis was

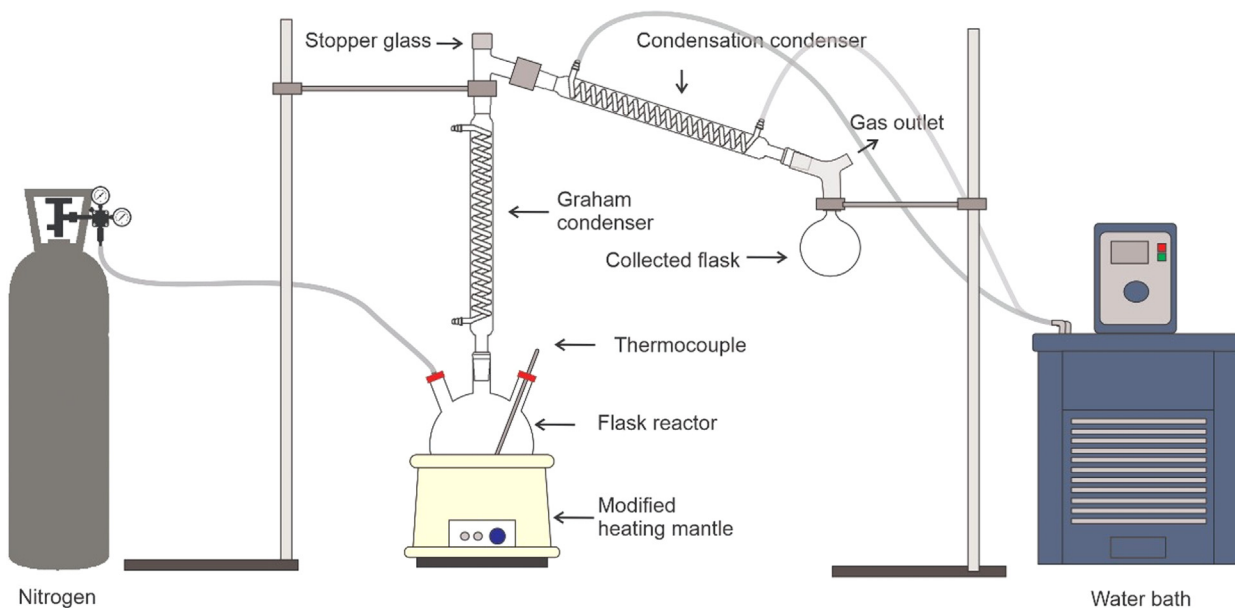


Fig. 1 Fractionated cracking set up for DO reaction.

carried out in accordance to the pre-established American Society for Testing and Materials (ASTM) standard. The pyrolysis oil density was measured with pycnometer using ASTM D 4052-09 standard, and dynamic viscosity was measured using the Fenske routine viscometer type of tube model 150 L938 (ASTM D 445-09). The acid value was tested by simple titration using ASTM 974-08e1 standard. Cloud and pour points were tested by a Petrotest machine using standard ASTM D 2500 – 66 and ASTM D97-87, respectively.

3. Results and discussion

3.1. Phase change analysis

Fig. 2 shows the XRD pattern of undoped dolomite, CMD900, and that with dopant catalysts (Fe/CMD900, Co/CMD900, Ni/CMD900, Cu/CMD900, and Zn/CMD900) after calcination at 900 °C for 4 h. The XRD pattern of calcined CMD900 was mainly composed of CaO and MgO. The intensified peaks that corresponded to CaO at 2θ were 32.4°, 37.6°, 54.1°, 64.3°, and 67.6° (JCPDS File: 37-1497) and MgO peaks at 2θ were 43.1°, 62.5°, 74.9°, and 78.8° (JCPDS File: 71-1176), which were in agreement with those in (Zhou et al., 2017). The high intensities of the diffractograms indicated the high crystallinity of CaO–MgO. The characteristic diffraction peaks of Fe/CMD900 exhibited at 2θ were 44.6°, 58.2°, and 77.1° (JCPDS File: 01-089-6466). For Co/CMD900, the major phases of CoO at 2θ were 34.5° and 77.2° (JCPDS File: 01-042-1300). For Ni/CMD900, the diffraction pattern clearly observed at 2θ were 43.2° and 48.5° (JCPDS File: 01-089-5881). The characteristic CuO peaks observed 2θ were 37.6°, 43.8°, and 51.2° (JCPDS File: 01-077-1898). A peak in the Zn/CMD900 pattern corresponded to ZnO, which was slightly

observed at $2\theta = 37.8^\circ$ and 48.6° (JCPDS File: 01-036-1451). The result shows that the reflection peaks of CaO and MgO were slightly shifted along with the reduction in intensity with the presence of metal oxide that was well dispersed onto the CMD900 (Shajaratun Nur et al., 2014). This finding was consistent with the crystallinity calculation, in which the crystallite size of the modified dolomite catalyst was slightly altered after loading with transition metal (Table 2).

The average crystallite sizes of the CMD900 and all doped CMD900 samples were estimated by Debye–Scherer’s equation based on the significant peaks of CaO and MgO (Table 2). The crystallite sizes of doped CDM900 were in the order of Fe/CMD900 > Zn/CMD900 > Ni/CMD900 > Co/CMD900 > Cu/CMD900 > CMD900. The average crystallite size increase upon the addition of metal oxide resulted in the expansion of the crystalline structure.

The specific surface area, pore volume, and average pore size for CMD900 and doped CMD900 catalysts with various transition metals are presented in Table 2. The surface area of CMD900 was 12.02 m²/g. Meanwhile, all the doped CMD900 catalysts show the least improvement in terms of textural properties because the surface area has a low porous structure. The surface area was in the order of Fe/CMD900 > Cu/CMD900 > Zn/CMD900 > Ni/CMD900 > Co/CMD900 > CMD900. The low surface area of all synthesised catalysts might be caused by the sintering effect of the catalyst after calcination, which can create severe particle agglomeration (Waheed et al., 2016). Table 2 reveals that the pore sizes in CMD900 are macroporous (e.g., 63.07 nm). Nevertheless, the pore diameter of all doped CMD900 catalysts exhibited slight reduction, and they mainly consisted of mesoporous structure with a pore diameter that was within the range of 2–50 nm, except for Co/CMD900, which was still in the macroporous range size (Shajaratun Nur et al., 2014). The

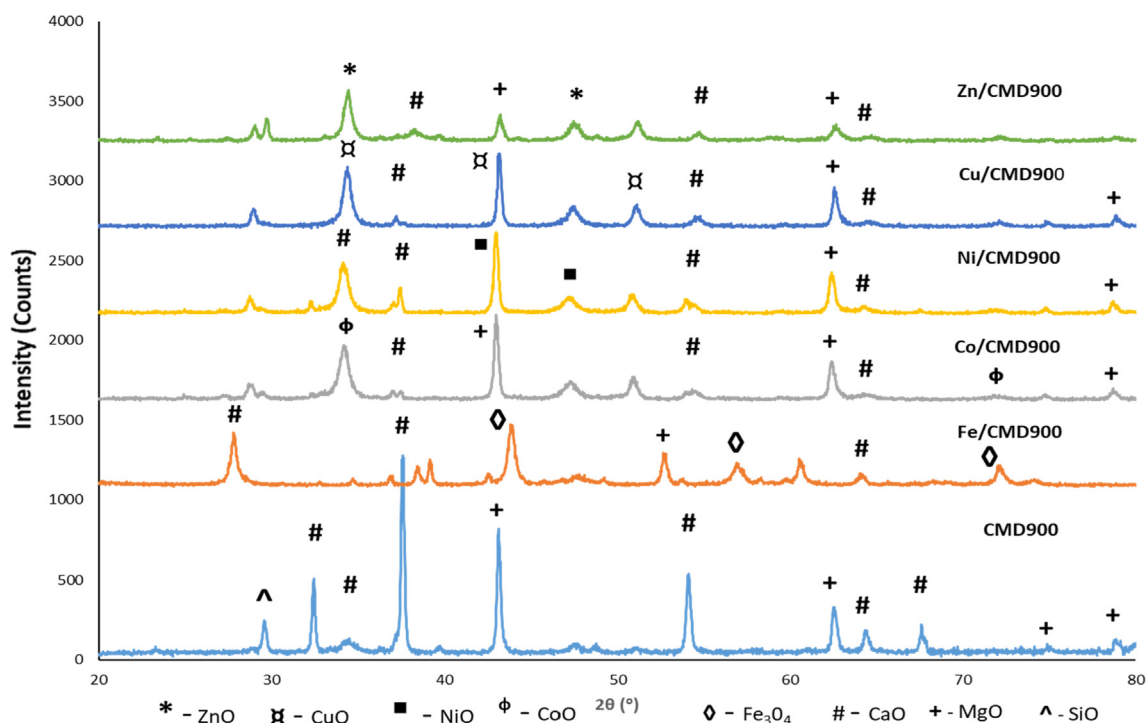


Fig. 2 XRD pattern of CMD900 and transition metal doped CMD900 catalysts.

Table 2 Physicochemical properties of the catalysts.

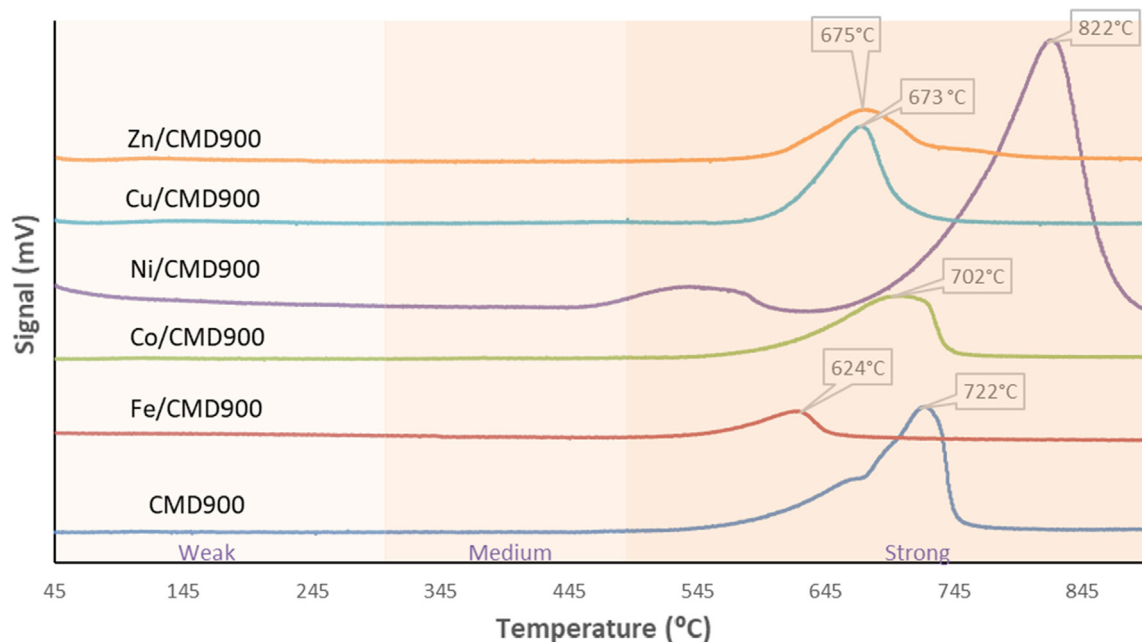
Characterisation	Crystallite size (nm)	BET surface area (m ² /g)	Pore volume (cm ³ /g)	Average pore diameter (nm)	Amount of desorbed CO ₂ (μmol/g)
CMD900	49.51	12.02	0.24	63.07	2872.73
Fe/CMD900	24.53	51.03	0.29	22.56	488.20
Co/CMD900	90.68	16.08	0.23	56.58	1776.78
Ni/CMD900	50.37	18.22	0.22	48.20	7306.37
Cu/CMD900	113.42	26.40	0.21	31.38	1826.59
Zn/CMD900	44.16	23.11	0.24	41.28	1213.85

pore size of all the synthesised catalysts increase in the order of CMD900 > Co/CMD900 > Ni/CMD900 > Zn/CMD900 > Cu/CMD900 > Fe/CMD900. However, this increase can still provide a wide channel for the diffusion of reactant for the catalytic activity (Asikin-Mijan et al., 2018). In addition, the reduction of pore volume after dispersion with metal dopant onto CMD900, except Fe/CMD900, were shown in Table 2. The trend of the pore volume was presented as follows: Fe/CMD900 > CMD900 > Zn/CMD900 > Co/CMD900 > Ni/CMD900 > Cu/CMD900. The decrement in pore size might be due to the pore blockage caused by the metal dopant particles that filled inside the CMD900 pore (Waheed et al., 2016).

The basicity characteristic of all synthesised catalysts was summarised in Table 2 and Fig. 3. The basicity trend was increased in the order of Ni/CMD900 > CMD900 > Cu/CMD900 > Co/CMD900 > Zn/CMD900 > Fe/CMD900. The transition metal doped CMD900 catalyst (except Ni/CMD900) showed low intensity on CO₂ desorption peaks at low temperature (624 °C to 702 °C) when compared with the CMD900 catalyst (Table 2 and Fig. 3). This finding suggested that the presence of a considerable amount of weak acid sites on the CMD900 catalyst surface was due to the successful dispersion of 5 wt% of transition metals on the CMD900 catalyst

surface. According to Asikin-Mijan et al. (2018) the presence of acid sites was attributed to the Bronsted acid sites associated with the bridging of OH groups and/or the Lewis acid sites associated with the presence of transition metal ions. The TPD profiles of CMD900 and all doped CMD900 catalysts shown in Fig. 3 exhibited considerably high basic strength with CO₂ desorption peak at a temperature of more than 500 °C. The basic strength distribution from the catalyst active sites is expressed in terms of CO₂ desorption temperature. The basic strength ($T_{max} = 822$ °C) and basic density (7306.37 μmol/g) of Ni/CMD900 catalyst significantly increased because of the synergy effect promoted by the interaction between NiO-CaO/MgO and the increment in active sites that resulted from the dispersion of NiO on the CMD900 surface. The characteristic of basicity is important to inhibit coke formation and enhance the cracking reaction (Kay Lup et al., 2017).

The morphological features of CMD900 and doped CMD900 catalysts at 60,000× magnification were shown in Fig. 4. The SEM images of CMD900 showed an agglomeration structure of particles and appeared in finer and smaller uniform sizes because of the sintering effect of metal oxides during calcination. The individual grain's segregation can be clearly observed and identified. However, the SEM morphology of the active metal-doped catalyst rendered significant

**Fig. 3** TPD-CO₂ profile for CMD900 and transition metal-doped CMD900 catalysts.

changes in morphology for surface structure into larger irregular aggregate and rough surface. The active metal-doped catalysts also displayed a more agglomerated structure, which indicates well-dispersed metal oxide on the dolomite catalyst surface. The segregated grains of dolomite become increasingly invisible. As evidence, the crystallite size of active metal-doped catalysts increased with the dispersion of transition metals, thereby implying the growth of the catalyst crystal. A similar observation was reported by [Azri et al. \(2020\)](#) when metal was added to dolomite as an effective catalyst for glycerol hydrogenolysis. In addition, the active metal-doped catalysts comprised small cluster, which resulted in high surface area of the catalyst ([Table 2](#)).

3.2. Catalyst performance in catalytic pyrolysis reaction of WCO

The conversion of WCO and WCO deoxygenated product distribution for all synthesised catalyst are shown in [Fig. 5](#). The conversion of WCO followed the sequence: Ni/CMD900 > Fe/CMD900 > Co/CMD900 > Zn/CMD900 > Cu/CMD900 > CMD900. The DO of WCO will lead to the production of the liquid product via decarboxylation and decarbonylation with the release of gas and acid phase as the by-products, respectively. The liquid products obtained from all DO reactions were divided into two separate fractions, namely, pyrolysis oil and acid phase with insignificant soap formation. The pyrolysis oil produced were in the order of Ni/CMD900 > Zn/CMD900 > Fe/CMD900 > Co/CMD900 > Cu/CMD900 > CMD900. This finding shows that TMO is a good promoter and has played an important role in tuning product selectivity towards monofunctional hydrocarbon intermediates, which further converted into the desired liquid product (pyrolysis oil).

The acid phase composed of water and a high amount of carboxylic compound was detected at the bottom phase of the liquid product. This finding suggested that the decarboxylation reaction was more preferred than the decarbonylation reaction. Ni/CMD900 catalyst produced a lesser amount of acid phase (0.1%) in the liquid product as compared with other catalysts. Nevertheless, white precipitate, (or soap) was observed in all liquid products catalysed by doped CMD900 catalysts. Ni/CMD900 shows the lowest amount of soap formed (6.7%) but still slightly higher than the un-doped CMD900 catalyst (4.8%). Supposedly, the formation of undesirable by-product (coke) must be avoided during the DO reaction for an ideal reaction. However, all the reactions with all catalysts tested yielded substantial coke formation in the following order: CMD900 > Cu/CMD900 > Zn/CMD900 > Co/CMD900 > Fe/CMD900 > Ni/CMD900. [Asikin-Mijan et al. \(2018\)](#) reported that the coke generated via polymerisation reaction in the DO of triolein was expected to occur because of the poor acidic properties of active-doped metal catalyst in CaO surface. The mass balance profile suggested that Ni/CMD900 catalyst can perform actively for the DO reaction of WCO because of the high amount of basic site on the catalyst surface ([Table 1](#)). Based on a previous study ([Romero et al., 2016](#)), the composition of gas produced via DO of WCO was analysed using GC-TCD. The gas was collected for certain reaction time at a certain temperature, and the gaseous product consisted of hydrocarbon gas, CO₂, CO, CH₄, H₂ and O₂ (except calcined dolomite), using various catalysts, such as calcined Malaysian dolomite and commercial acid catalyst (e.g. FCC, Zeolite NaY, HZSM-5).

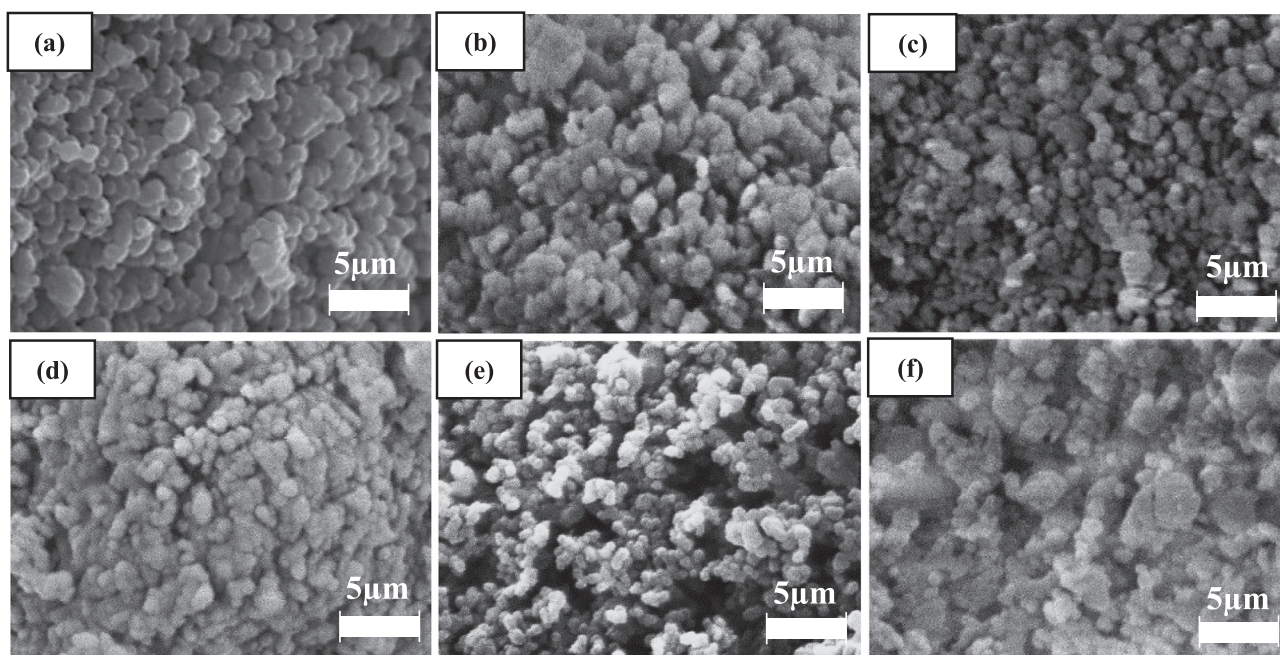


Fig. 4 Morphology of (a) CMD900, (b) Fe/CMD900, (c) Co/CMD900, (d) Ni/CMD900, (e) Cu/CMD900 and (f) Zn/CMD900 catalysts at 60 k magnification.

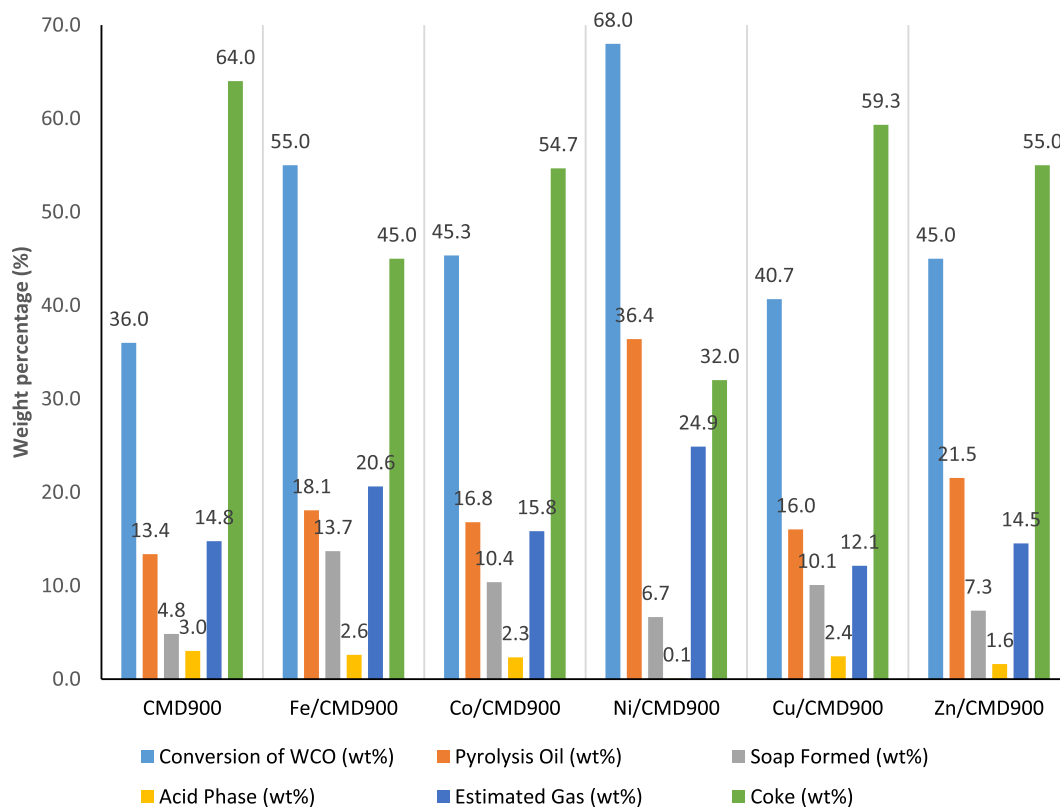


Fig. 5 Product distribution in DO of WCO by various catalyst dopant on CMD900.

3.3. Characterisation of liquid product using GC–MS analysis

3.3.1. Chemical composition

Fig. 6 shows the main composition determined by GC–MS analysis for the produced pyrolysis oil catalysed by all synthesised catalysts with different catalyst dopants. This study showed that WCO was thermally cracked to a liquid hydrocarbon product and a small quantity of oxygenated compounds. As shown in Fig. 6, the trend of liquid hydrocarbon yield was in the order of Ni/CMD900 > CMD900 > Co/CMD900 > Fe/CMD900 > Zn/CMD900 > Cu/CMD900. The oxygenated compound yielded in the following order: Cu/CMD900 > Zn/CMD900 > Fe/CMD900 > Co/CMD900 > CMD900 > Ni/CMD900. Based on these findings, the DO performance of Ni/CMD900 resulted in the highest yield of liquid hydrocarbon and the lowest yield of the oxygenated compound, suggesting that the synergistic energy effect from acid–base interaction between NiO and CaO–MgO performed actively in the DO of WCO as mixed metal oxides. NiO improved the yield production of liquid products comprising mainly hydrocarbons, thereby presenting a potentially high-value chemical feedstock or fuel source. Based on Fig. 6, CMD900 catalyst contains the unique basic properties of CaO–MgO, which helps in oxygen removal by absorbing more CO₂ in the gas phase. This finding is line with the result shown by Lin et al. (2010) in the pyrolysis of biomass using dolomite (MgO–CaO) catalyst as related to the reduction of tar formation with the increase in H/C ratio. The observation showed that the presence of MgO and CaO will produce a better route for oxygen removal through catalytic DO. The reduction in

oxygenated compounds in pyrolysis oil product by synthesised Ni/CMD900 catalysts were also due to the existence of a large density of basic site Ni-promoted catalyst (4.40×10^{21} atom/g) as compared with other metal-promoted catalysts and hence improved catalyst stability during DO reaction. The efficiency of DO reaction has been calculated on the basis of the reduction of oxygenated compound present in pyrolysis oil generated using synthesised transition metal-doped dolomite catalyst through area of GC–MS analysis data (Eq. (5)). The trend of oxygenated compound removal was in the order of Ni/CMD900 (79.8%) > CMD900 (76%) > Co/CMD900 (71.9%) > Fe/CMD900 (67.9%) > Zn/CMD900 (65.6%) > Cu/CMD900 (62.4%). This finding showed that the catalysts can reduce oxygenated compound via desired catalytic DO pathway whilst improving the quality of the final fuel product. Based on Zhang et al. (2016), strong basic site generated from oxygen on the metal oxides created stronger forces via the abstraction of alpha hydrogen in carbonyl compound and followed by C–O scission to form hydrocarbon compound.

Fig. 7 shows a formation of a high number of oxygenated by-products, such as alcohol and carboxylic acid. Fe/CMD900, Cu/CMD900, Co/CMD900 and Zn/CMD900 are amongst the catalysts with high alcohol value (e.g. 15.1%, 13.8%, 13.8% and 7.1%, respectively). For carboxylic acid, the alcohol value of the aforementioned catalysts is 4.6%, 11.0%, 5.4% and 11.7%, respectively. Ni/CMD900 catalyst contains less carboxylic acid (3.6%) with a minor quantity of ketone (2.6%), and the absence of aldehydes indicates a slight occurrence of such oxidation reaction in the DO reaction as compared with other transition metal-promoted catalysts. High acid value was obtained with presence of high amount

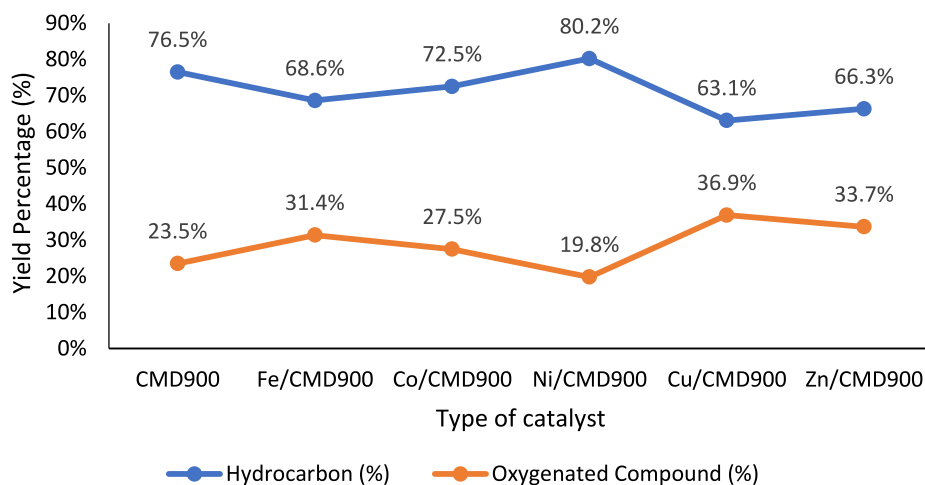


Fig. 6 Main product composition in pyrolysis oil produced according to the catalyst dopant.

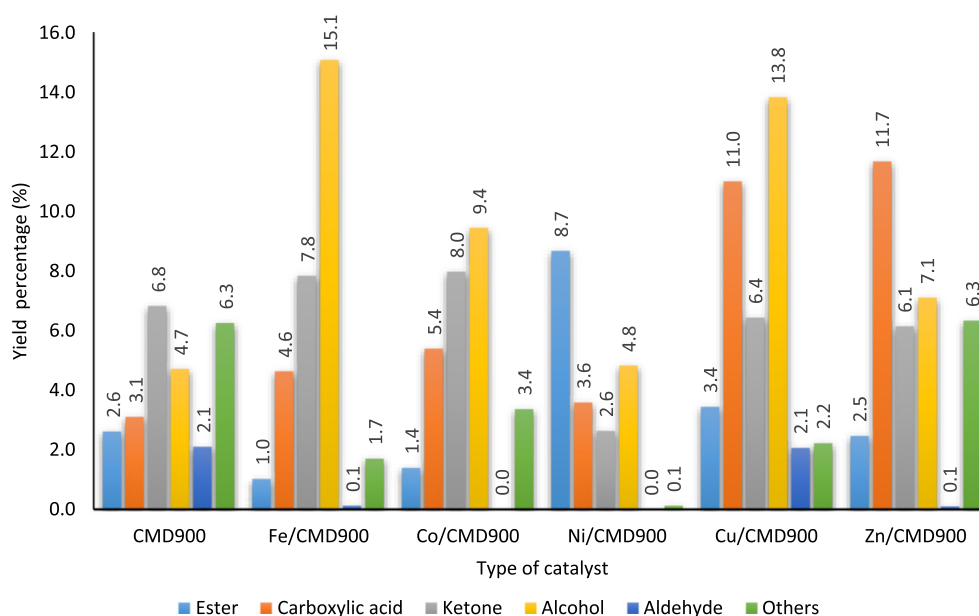


Fig. 7 Chemical groups of oxygenated compounds in pyrolysis oil produced according to the catalyst dopant.

of carboxylic acid group in the oxygenated compound. The produced pyrolysis oil contains a lower acid value with the presence of these catalysts, starting with CMD900 (33 mg KOH/ g) followed by Fe/CMD900 (40 mg KOH/ g) < Ni/CMD900 (47 mg KOH/ g) < Co/CMD900 (64 mg KOH/ g) < Cu/CMD900 (75 mg KOH/ g) < Zn/CMD900 (78 mg KOH/ g) as compared with the 186 mg KOH/g acid value of pyrolysis oil generated from non-catalytic WCO pyrolysis (Hafriz et al., 2018). The presence of transition metals doped on dolomite catalyst increased the acid value of pyrolysis oil produced as compared with the CMD900 catalyst. This phenomenon is in accordance with the low reduction of carboxylic acid upon the incorporation of transition metals on CMD900. Other researchers have suggested that carboxylic acid groups are more difficult to hydrogenate with a present

transition metal relative to other functional types in bio-oil, such as ketone, aldehyde carbonyls and alkenes (Laurent et al., 1999). As reported by Li et al. (2013), lower acid value had relationship with good cold flow properties, such as the cold filter plugging point and freezing point.

Fig. 8 presents the further breakdown of the main compounds into individual chemical groups, as determined by GC-MS analysis pyrolysis oil produced for CMD900 and transition metal-doped CMD900 catalyst. The main chemical groups can be classified into seven components according to their structure, namely, alkanes, cycloalkane, alkene, cycloalkene, diene, alkyne, and aromatic. The figure shows that the hydrocarbon product is dominated by aliphatic hydrocarbon, namely, alkene and alkane, for all synthesised catalysts. Evidently, aliphatic alkene was dominating the composition as

compared with alkane in this liquid product with the order of Ni/CMD900 > Co/CMD900 > CMD900 > Fe/CMD900 > Zn/CMD900 > Cu/CMD900. Meanwhile, the aliphatic alkane yielded in the following order: Ni/CMD900 > Co/CMD900 > Zn/CMD900 > Fe/CMD900 > CMD900 > Cu/CMD900. In the case of Ni/CMD900 catalyst, the highest concentration in alkane was detected as tetradecane (C₁₄H₃₀) and tridecane (C₁₃H₂₈).

Meanwhile, 8-heptadecene (C₁₇H₃₈) and 1-tridecene (C₁₃H₂₆) were the most abundant in alkene. The aliphatic alkane for Fe/CMD900, Zn/CMD900 and Cu/CMD900 were mostly tetradecane and tridecane, except in Mo/CMD900, in which tetradecane and dodecane (C₁₂H₂₆) were detected in the produced pyrolysis oil. The alkenes present for all tested metals promoted catalysts and were mostly from 8-heptadecene and 1-tridecene. The detailed characterisation of hydrocarbon fractions distribution for the deoxygenated liquid product conversion (Fig. 9) showed that the hydrocarbon fractions for Ni/CMD900 catalyst was composed of a mixture of n-C₁₄ and n-C₁₇. Meanwhile, Co/CMD900 catalyst contained n-C₁₄ and n-C₁₀ fractions. Zn/CMD900 and Fe/CMD900 were mostly composed by n-C₁₃ and n-C₁₂, whereas Cu/CMD900 contained the shortest C range, which was n-C₁₃ and n-C₁₀.

3.3.2. Product selectivity

Fig. 10 shows the composition of biofuel as determined by the carbon number of the gasoline, kerosene and diesel fraction as the petroleum product. Interestingly, CMD900 catalyst exhibits a high degree of selectivity (48.9%) of gasoline range (C₄-C₁₂). Doped CMD900 catalyst for gasoline fraction were presented in the following order: CMD900 > Co/CMD900, Fe/CMD900 > Cu/CMD900 > Ni/CMD900 > Zn/CMD900. However, catalytic DO over Ni/CMD900 catalyst were

found predominantly selective towards diesel range (55.2%) when compared with other doped metal in the order of Ni/CMD900 > Zn/CMD900 > Co/CMD900 > Fe/CMD900 > Cu/CMD900 > CMD900. In addition, Ni/CMD900 also shows higher fraction towards kerosene (38.8%). The DO reactivity towards kerosene was in the order of Ni/CMD900 > CMD900 > Co/CMD900 > Fe/CMD900 > Zn/CMD900 > Cu/CMD900.

3.4. Analysis of pyrolysis oil properties

The properties of the pyrolysis oil derived from Ni/CMD900 were investigated, and the results are shown in Table 3. For comparison purposes, Table 3 also displays the specified values for the pyrolysis oil (palm oil), diesel and hydrocarbon biofuel. The results show that the fuels derived from WCO using Ni/CMD900 as catalysts possessed acceptable values for the given properties when compared with other fuels, excluding the comparison of acid value with diesel. Acid value is referred to as the oil quality indicator to monitor the oil degradation during the storage period. According to the ASTM standard for fuel application, the maximum value of acid number is 0.5 mgKOH/g (Yasin et al., 2013). The number of the acid value of pyrolysis oil is high, and pyrolysis oil can be degraded at extensive storage period when compared with mineral diesel. Therefore, studies on reducing the acid value of pyrolysis oil can be conducted by modifying the synthesised catalyst and the ratio of blending with diesel in the future. However, Ni/CMD900 is an excellent low-cost catalyst for the DO of WCO; its typical bifunctional (NiO-CaO/MgO) properties could focus on the distribution of the product and improved the fuel properties.

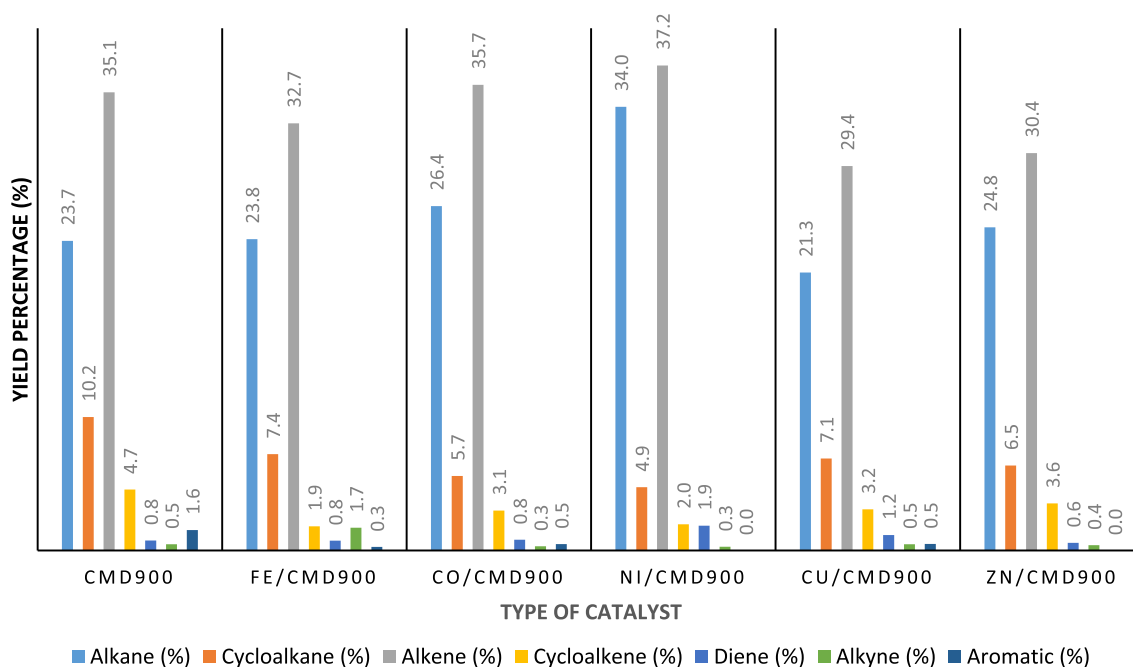


Fig. 8 Chemical groups of hydrocarbon compound in pyrolysis oil produced according to the catalyst dopant.

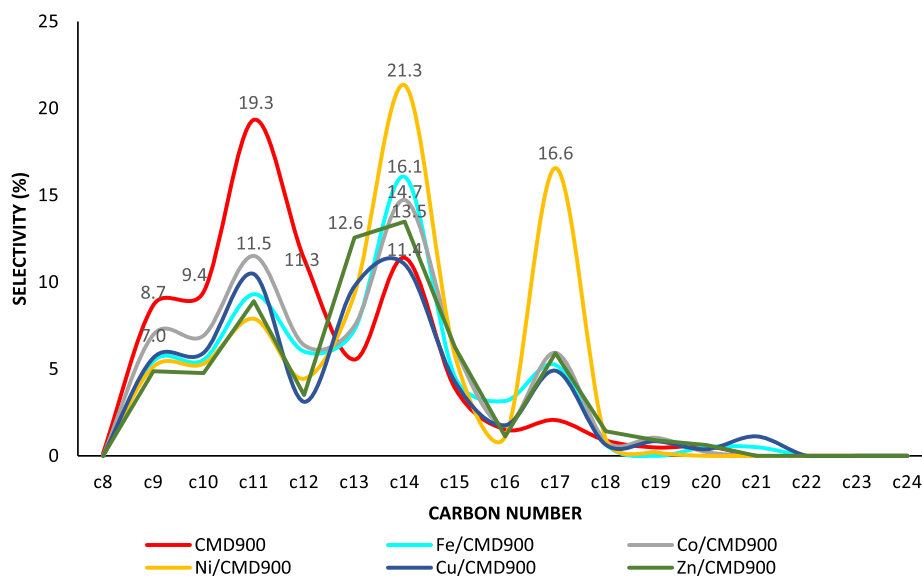


Fig. 9 Selectivity in hydrocarbon chain length from C8–C24.

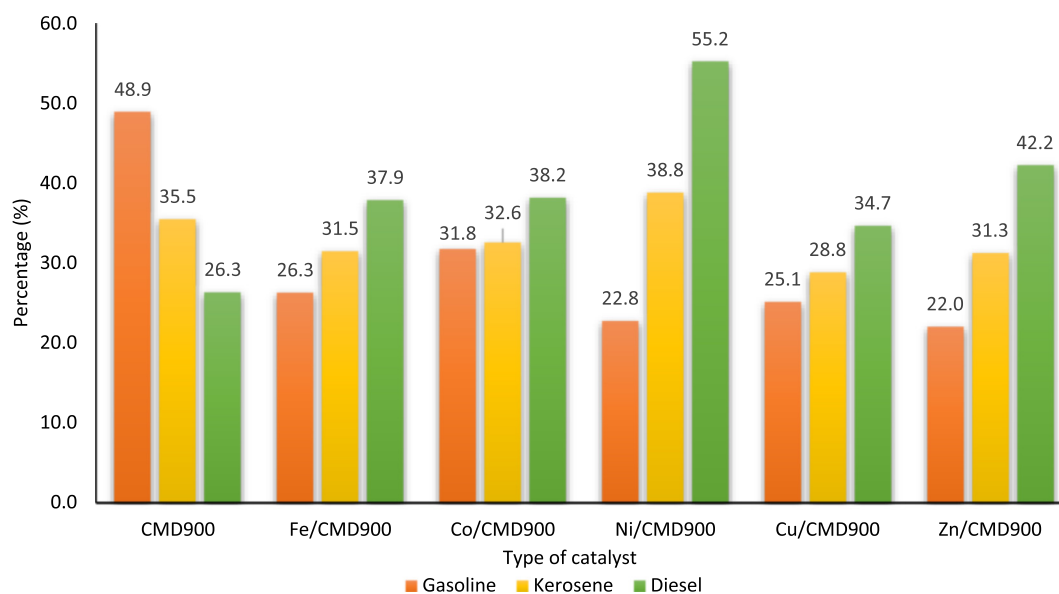


Fig. 10 Composition of biofuel in the produced pyrolysis oil.

Table 3 Physical and chemical properties of pyrolysis oil and diesel fuel.

No.	Parameter	Test method	Pyrolysis oil (Ni/CMD900)	Pyrolysis oil (Palm)	Diesel fuel	Hydro-carbon biofuel ^{a,c}
1.	Density (kg/m ³)	ASTM D 4052	811	818.4 ^d	836-850 ^c	760–880
2.	Kinematic viscosity (40 °C) (cSt)	ASTM D 445	2.19	2.7 ^c –3.2 ^f	2–8 ^c	1.45–4.22
3.	Acid Number (mgKOH/g)	ASTM D 974	47	58 ^f	3.2 ^f	33
4.	Cloud Point (°C)	ASTM D 2500	12	–8 ^f	13	–5 until –30
5.	Pour Point (°C)	ASTM D 97	–24	–22 ^f	–6 ^a until –20 ^e	9

Source: ^aMa and Hanna (1999); ^bLi et al. (2013); ^cPramanik et al. (2003); ^dLima et al. (2004); ^eKumar Tiwari et al. (2007); ^fXu et al. (2010).

3.5. Reaction mechanisms

The distribution and composition of the product were obtained through mass balance and GC–MS analysis, respectively. The general catalytic pyrolysis of WCO pathway under atmosphere free oxygen over modified Malaysian dolomite catalysts can be established in Fig. 11, as adapted from Lestari et al. (2009). The reaction pathways consist of liquid hydrocarbon, gas and solid and soap phase reactions. The liquid phase reactions of the WCO DO process dominantly involve decarboxylation and decarbonylation reactions to produce alkanes and alkenes by releasing carbon dioxide, carbon monoxide and water, as illustrated in Reactions (1) and (2) (Hafriz et al., 2018; Kamil et al., 2020; Snare et al., 2008). Based on Reaction (3), the triglyceride of WCO also undergone hydrogen abstraction at higher temperatures to produce diene formation. Meanwhile, alkenes and diene will also undergo Diels–Alder reaction to produce cycloalkenes, as shown in Reaction (4). Idem et al. (1996) mentioned that cycloalkenes are the main hydrocarbons used for synthesising the cycles and aromatic hydrocarbons. In a hydrogenation reaction (Reaction (5)), two hydrogen atoms are added across the double bond of cycloalkenes, thereby resulting in a stable form product called saturated cycloalkanes. A side reaction, such as dehydrogenation, could occur during the removal of

hydrogen from of cycloalkenes and alkenes to produce a small amount of aromatic and alkynes in a liquid hydrocarbon product, as mentioned in Reaction 6.

Gas is a secondary product that is generated via the DO of WCO. According to Idem et al. (1996), the hydrocarbon radicals R^u or R^s are formed by eliminating of ethylene molecules during secondary cracking. The straight and branched-chain hydrocarbons of which in the C_1 – C_5 range in the gas phase product were yielded through the successive elimination of ethylene molecules from the saturated and unsaturated hydrocarbon radicals followed by disproportionation, isomerisation, and subsequent hydrogen transfer reactions, as illustrated in Reaction 7. Dandik and Aksoy (1998) reported that the gaseous product generated from the catalytic pyrolysis of canola oil consisted mostly of hydrocarbon gases in the C_1 – C_5 range. In addition, the methanation reaction (Reaction 8) could occur as a pathway because of the conversion of carbon monoxide and carbon dioxide to methane (CH_4) through hydrogenation. In a review of the DO of fatty acid Hermida et al. (2015) also mentioned the water gas shift in Reaction 9 due to the presence of carbon monoxide and water via decarbonylation reaction in producing hydrogen and carbon dioxide.

Solid and soap phase reactions are the side reactions involved. In the solid-phase reaction, the polymerisation of

Liquid hydrocarbon (HCs) phase reactions:

- | | |
|--------------------------|---|
| 1. Decarboxylation; | $R-COOH \rightarrow C_n-H_{2n+2}$ (Alkanes) + CO_2 |
| 2. Decarbonylation; | $R-COOH \rightarrow C_n-H_{2n}$ (Alkenes) + CO + H_2O (acid phase) |
| 3. Hydrogen Abstraction; | $R-COOH \rightarrow R'=R$ (Dienes) |
| 4. Diels Alder Reaction; | C_n-H_{2n} (Alkenes) + $R'=R \rightarrow C_n-H_{2n-2}$ (cycloalkenes) |
| 5. Hydrogenation; | $C_n-H_{2n-2} + H_2 \rightarrow C_n-H_{2n}$ (cycloalkanes) |
| 6. Dehydrogenation; | $C_n-H_{2n-2} \rightarrow C_n-H_n$ (Aromatic HCs) + $2H_2$ |
| | $C_n-H_{2n} \rightarrow C_n-H_{2n-2}$ (alkynes) + $2H_2$ |

Gas-phase reactions:

- | | |
|--|---|
| 7. Ethylene elimination, isomerization, and hydrogen transfer reactions; | $R^u=R^s \rightarrow$ hydrocarbon gases (C_1 – C_5) |
| 8. Methanation; | $CO_2 + 4H_2 \rightleftharpoons CH_4 + 2H_2O$ |
| | $CO + 3H_2 \rightleftharpoons CH_4 + H_2O$ |
| 9. Water-gas shift; | $CO + H_2O \rightleftharpoons H_2 + CO_2$ |

Solid phase reactions:

- | | |
|---------------------|---|
| 10. Polymerization; | C_n-H_n (Aromatic HCs) \rightarrow Coke |
| 11. Condensation; | WCO \rightarrow Coke |

Soap Phase reaction:

- | | |
|---------------------|--|
| 12. Saponification; | $CaO + CO_2 \rightarrow CaCO_3$ |
| | $R-COOH + CaCO_3 \rightarrow Ca(RCOO)_2$ (F.A. soap) + CO_2 + H_2O |

Fig. 11 General catalytic pyrolysis of WCO pathway under atmosphere free oxygen over transition metal-doped calcined Malaysian dolomite catalyst.

aromatic hydrocarbon and the condensation of WCO generate the coke formation, as mentioned in Reactions 10 and 11, respectively. In the soap phase reaction, calcium carbonate is produced during the absorption of CO₂ by CaO because of the high formation of CaO composition in calcined Malaysian dolomite. The oxygenates, such as carboxylic acid (RCOOH), are expected to react with calcium carbonate (CaCO₃) in producing fatty acid soap (Ca(RCOO)₂), as illustrated in Reaction 12.

4. Conclusions

This study demonstrated that the calcined Malaysian dolomite (CMD900) was successfully dispersed with various transition metals, such as Fe, Co, Ni, Cu and Zn. The result indicated that amongst all of the doped catalyst, Ni/CMD900 catalyst demonstrated the best performance in terms of the DO reaction of WCO with high conversion (68.0%), high yield pyrolysis oil (36.4%) and low coke formation (32.0%). The high availability of active basic sites on the Ni/CMD900 catalyst surface plays an important role in affecting the catalytic behaviour in the DO reaction of WCO. CMD900 can also remove high oxygen content with only 19.8% of oxygenated compound detected and produced the maximum yield of hydrocarbon product (80.2%) of C₁₃ and C₁₇ fractions. In addition, Ni/CMD900 catalysed reaction rendered higher selectivity towards diesel when compared with other doped CMD900 catalysts.

Declaration of Competing Interest

The authors declare that they have no known competing financial interests or personal relationships that could have appeared to influence the work reported in this paper.

Acknowledgement

The authors acknowledge the financial support from the Ministry of Higher Education of Malaysia for Fundamental Research Grant Scheme (FRGS/11/TK/UPM/02) and AAIBE Chair of Renewable Energy Grant No. 201801 KETTHA for funding this research publication.

References

- Alsultan, G.A., Asikin-mijan, N., Lee, H.V., Albazzaz, A.S., 2017. Deoxygenation of waste cooking to renewable diesel over walnut shell-derived nanorod activated carbon-supported CaO-La₂O₃ catalyst. *Energy Convers. Manag.* 151, 311–323. <https://doi.org/10.1016/j.enconman.2017.09.001>.
- Arstad, B., Lind, A., Andreassen, K.A., Pierchala, J., Thorshaug, K., Blom, R., 2014. In-situ XRD studies of dolomite based CO₂ sorbents. *Energy Proc.* 63, 2082–2091. <https://doi.org/10.1016/j.egypro.2014.11.224>.
- Asikin-Mijan, N., Lee, H.V., Taufiq-Yap, Y.H., Juan, J.C., Rahman, N.A., 2016. Pyrolytic-deoxygenation of triglyceride via natural waste shell derived Ca(OH)₂nanocatalyst. *J. Anal. Appl. Pyrol.* 117, 46–55. <https://doi.org/10.1016/j.jaap.2015.12.017>.
- Asikin-Mijan, N., Lee, H.V., Marliza, T.S., Taufiq-Yap, Y.H., 2018. Pyrolytic-deoxygenation of triglycerides model compound and non-edible oil to hydrocarbons over SiO₂-Al₂O₃ supported NiO-CaO catalysts. *J. Anal. Appl. Pyrol.* 129, 221–230. <https://doi.org/10.1016/j.jaap.2017.11.009>.
- Asikin-Mijan, N., Lee, H.V., Abdulkareem-Alsultan, G., Afandi, A., Taufiq-Yap, Y.H., 2018. Production of green diesel via cleaner catalytic deoxygenation of *Jatropha curcas* oil. *J. Clean. Prod.* 167, 1048–1059. <https://doi.org/10.1016/j.jclepro.2016.10.023>.
- Azri, N., Ramli, I., Nda-Umar, U.I., Shamsuddin, M.R., Saiman, M. I., Taufiq-Yap, Y.H., 2020. Copper-dolomite as effective catalyst for glycerol hydrogenolysis to 1,2-propanediol. *J. Taiwan Inst. Chem. Eng.* <https://doi.org/10.1016/j.jtice.2020.07.011>.
- Ben Hassen Trabelsi, A., Zaafour, K., Baghdadi, W., Naoui, S., Ouerghi, A., 2018. Second-generation biofuels production from waste cooking oil via pyrolysis process. *Renew. Energy* 126, 888–896. <https://doi.org/10.1016/j.renene.2018.04.002>.
- Chang, J.-S., Cheng, J.-C., Ling, T.-R., Chern, J.-M., Wang, G.-B., Chou, T.-C., 2017. Low acid value bio-gasoline and bio-diesel made from waste cooking oils using a fast pyrolysis process. *J. Taiwan Inst. Chem. Eng.* 73, 1–11. <https://doi.org/10.1016/j.jtice.2016.04.014>.
- Charusiri, W., Vitidsant, T., 2017. Upgrading bio-oil produced from the catalytic pyrolysis of sugarcane (*Saccharum officinarum* L) straw using calcined dolomite. *Sustain. Chem. Pharm.* 6, 114–123. <https://doi.org/10.1016/j.scp.2017.10.005>.
- Chen, G., Liu, C., Ma, W., Zhang, X., Li, Y., Yan, B., 2014. Biosource Technology Co-pyrolysis of corn cob and waste cooking oil in a fixed bed 166, 500–507.
- Choi, I.H., Lee, J.S., Kim, C.U., Kim, T.W., Lee, K.Y., Hwang, K.R., 2018. Production of bio-jet fuel range alkanes from catalytic deoxygenation of *Jatropha* fatty acids on a WO_x/Pt/TiO₂catalyst. *Fuel* 215, 675–685. <https://doi.org/10.1016/j.fuel.2017.11.094>.
- Dandik, L., Aksoy, H.A., 1998. Pyrolysis of used sunflower oil in the presence of sodium carbonate by using fractionating pyrolysis reactor. *Fuel Process Technology* 57, 81–92. [https://doi.org/10.1016/S0378-3820\(98\)00074-5](https://doi.org/10.1016/S0378-3820(98)00074-5).
- Dong, R., Zhao, M., 2018. Research on the pyrolysis process of crumb tire rubber in waste cooking oil. *Renew. Energy* 125, 557–567. <https://doi.org/10.1016/j.renene.2018.02.133>.
- Fazril, I., Shamsuddin, A.H., Nomanbhay, S., Kusomo, F., Hanif, M., Ahmad Zamri, M.F.M., Ismail, M.F., 2020. Microwave-assisted in situ transesterification of wet microalgae for the production of biodiesel: progress review. *IOP Conference Series: Earth Environ. Sci.* 476. <https://doi.org/10.1088/1755-1315/476/1/012078>.
- Hafriz, R.S.R.M., Salmiaton, A., Yunus, R., Taufiq-Yap, Y.H., 2018. Green biofuel production via catalytic pyrolysis of waste cooking oil using Malaysian dolomite catalyst. *Bull. Chem. React. Eng. Catal.* 13, 489–501. <https://doi.org/10.9767/bcrec.13.3.1956.489-501>.
- Hermida, L., Abdullah, A.Z., Mohamed, A.R., 2015. Deoxygenation of fatty acid to produce diesel-like hydrocarbons: A review of process conditions, reaction kinetics and mechanism. *Renew. Sustain. Energy Rev.* 42, 1223–1233. <https://doi.org/10.1016/j.rser.2014.10.099>.
- Idem, R.O., Katikaneni, S.P.R., Bakhshi, N.N., 1996. Thermal cracking of canola oil: reaction products in the presence and absence of steam. *Energy Fuels* 10 (6), 1150–1162. <https://doi.org/10.1021/ef00052a005>.
- Kamil, F., Ali, S., Hafriz Raja Shahruzzaman, R.M., Hussien, I., Omer, R., 2020. Characterization and application of molten slag as catalyst in pyrolysis of waste cooking oil. *Bull. Chem. React. Eng. Catal.* 15 (1), 119–127. <https://doi.org/10.9767/bcrec.15.1.3973.119-127>.
- Kay Lup, A.N., Abnisa, F., Wan Daud, W.M.A., Aroua, M.K., 2017. A review on reactivity and stability of heterogeneous metal catalysts for deoxygenation of bio-oil model compounds. *J. Ind. Eng. Chem.* 56, 1–34. <https://doi.org/10.1016/j.jiec.2017.06.049>.
- Kumar Tiwari, A., Kumar, A., Raheman, H., 2007. Biodiesel production from *Jatropha* oil (*Jatropha curcas*) with high free

- fatty acids: An optimized process. *Biomass Bioenergy* 31 (8), 569–575. <https://doi.org/10.1016/j.biombioe.2007.03.003>.
- Lam, S.S., Wan Mahari, W.A., Cheng, C.K., Omar, R., Chong, C.T., Chase, H.A., 2016. Recovery of diesel-like fuel from waste palm oil by pyrolysis using a microwave heated bed of activated carbon. *Energy* 115, 791–799. <https://doi.org/10.1016/j.energy.2016.09.076>.
- Laurent, E.; Pierret, C.; Grange, P.; Delmon, B. Control of the deoxygenation of pyrolytic oils by hydrotreatment. Proceedings of the 6th EC International Conference on Biomass for Energy 1999, Industry and Environment; Athens, Greece.
- Lestari, S., Maki-Arvela, P., Beltramini, J., Lu, G.Q.M., Murzin, D. Y., 2009. Transforming triglycerides and fatty acids into biofuels. *ChemSusChem* 2 (12), 1109–1119. <https://doi.org/10.1002/cssc.200900107>.
- Li, L., Quan, K., Xu, J., Liu, F., Liu, S., Yu, S., Ge, X., 2013. Liquid hydrocarbon fuels from catalytic cracking of waste cooking oils using basic mesoporous molecular sieves K2O/Ba-MCM-41 as catalysts. *ACS Sustain. Chem. Eng.* 1 (11), 1412–1416. <https://doi.org/10.1021/sc4001548>.
- Lima, D.G., Soares, V.C.D., Ribeiro, E.B., Carvalho, D.A., Cardoso, É.C.V., Rassi, F.C., Suarez, P.A.Z., 2004. Diesel-like fuel obtained by pyrolysis of vegetable oils. *J. Anal. Appl. Pyrol.* 71 (2), 987–996. <https://doi.org/10.1016/j.jaap.2003.12.008>.
- Lin, Y., Zhang, C., Zhang, M., Zhang, J., 2010. Deoxygenation of bio-oil during pyrolysis of biomass in the presence of CaO in a fluidized-bed reactor. *Energy Fuels* 24 (10), 5686–5695. <https://doi.org/10.1021/ef1009605>.
- Ma, F., Hanna, M.A. Biodiesel production: a review 1999. *Journal Series 12109, Agricultural Research Division, Institute of Agriculture and Natural Resources, University of Nebraska-Lincoln*. *Bioresource Technology*, 70(1), 1–15. doi: 10.1016/s0960-8524(99)00025.
- Mao, N., Zhou, C.H., Keeling, J., Fiore, S., Zhang, H., Chen, L., 2017. Tracked changes of dolomite into Ca-Mg-Al layered double hydroxide. *Appl. Clay Sci.* 159, 25–36. <https://doi.org/10.1016/j.clay.2017.06.011>.
- Mohammed, M.A.A., Salmiaton, A., Wan Azlina, W.A.K.G., Mohamad Amran, M.S., Taufiq Yap, Y.H., 2013. Preparation and characterization of Malaysian dolomites as tar cracking catalyst in biomass gasification process. *J. Energy* 791582, 8. <https://doi.org/10.1155/2013/791582>.
- Pattanaik, B.P., Misra, R.D., 2017. Effect of reaction pathway and operating parameters on the deoxygenation of vegetable oils to produce diesel range hydrocarbon fuels: A review. *Renew. Sustain. Energy Rev.* 73, 545–557. <https://doi.org/10.1016/j.rser.2017.01.018>.
- Pramanik, K., 2003. Properties and use of jatropha curcas oil and diesel fuel blends in compression ignition engine. *Renew. Energy* 28 (2), 239–248. [https://doi.org/10.1016/s0960-1481\(02\)00027-7](https://doi.org/10.1016/s0960-1481(02)00027-7).
- Romero, M.J.A., Pizzi, A., Toscano, G., Busca, G., Bosio, B., Arato, E., 2016. Deoxygenation of waste cooking oil and non-edible oil for the production of liquid hydrocarbon biofuels. *Waste Manag.* 47, 62–68. <https://doi.org/10.1016/j.wasman.2015.03.033>.
- Seifi, H., Sadrameli, S.M., 2016. Improvement of renewable transportation fuel properties by deoxygenation process using thermal and catalytic cracking of triglycerides and their methyl esters. *Appl. Therm. Eng.* 100, 1102–1110. <https://doi.org/10.1016/j.applthermaleng.2016.02.022>.
- Shahrzaman, R. M. H. Raja, Salmiaton, A. Yunus, R., Taufiq-Yap, Y.H., 2018. Modified local carbonate mineral as deoxygenated catalyst for biofuel production via catalytic pyrolysis of waste cooking oil. *AIP Conference Proc.* 2030(1), 020006. doi: 10.1063/1.5066647.
- Shajaratun Nur, Z.A., Taufiq-Yap, Y.H., Rabiah Nizah, M.F., Teo, S. H., Syazwani, O.N., Islam, A., 2014. Production of biodiesel from palm oil using modified Malaysian natural dolomites. *Energy Convers. Manag.* 78, 738–744. <https://doi.org/10.1016/j.enconman.2013.11.012>.
- Snare, M., Kubickova, I., Maki-Arvela, P., Chichova, D., Eranen, K., Murzin, D.Y., 2008. Catalytic deoxygenation of unsaturated renewable feedstocks for production of diesel fuel hydrocarbons. *Fuel* 87 (933–45). <https://doi.org/10.1016/j.fuel.2007.06.006>.
- Sousa, F.P., Silva, L.N., de Rezende, D.B., de Oliveira, L.C.A., Pasa, V.M.D., 2018. Simultaneous deoxygenation, cracking and isomerization of palm kernel oil and palm olein over beta zeolite to produce biogasoline, green diesel and biojet-fuel. *Fuel* 223, 149–156. <https://doi.org/10.1016/j.fuel.2018.03.020>.
- Waheed, Q.M.K., Wu, C., Williams, P.T., 2016. Pyrolysis/reforming of rice husks with a Ni e dolomite catalyst: influence of process conditions on syngas and hydrogen yield. *J. Energy Inst.* 89, 657–667. <https://doi.org/10.1016/j.joei.2015.05.006>.
- Wako, F.M., Reshad, A.S., Bhalerao, M.S., Goud, V.V., 2018. Catalytic cracking of waste cooking oil for biofuel production using zirconium oxide catalyst. *Ind. Crops Prod.* 118, 282–289. <https://doi.org/10.1016/j.indcrop.2018.03.057>.
- Wang, J., Zhong, Z., Zhang, B., Ding, K., Xue, Z., Deng, A., 2017. Upgraded bio-oil production via catalytic fast co-pyrolysis of waste cooking oil and tea residual. *Waste Manag.* 60, 357–362. <https://doi.org/10.1016/j.wasman.2016.09.008>.
- Xu, J., Jiang, J., Sun, Y., Chen, J., 2010. Production of hydrocarbon fuels from pyrolysis of soybean oils using a basic catalyst. *Bioresour. Technol.* 101 (24), 9803–9806. <https://doi.org/10.1016/j.biortech.2010.06.147>.
- Yasin, M. H. mat, Mamat, R., Yusop, A. F., Rahim, R., Aziz, A., Shah, L.A. Fuel physical characteristics of biodiesel blend fuels with alcohol as additives. *Proc. Eng.* 2013, 53, 701–706. doi: 10.1016/j.proeng.2013.02.091.
- Zhang, J., Wang, K., Nolte, M.W., Choi, Y.S., Brown, R.C., Shanks, B.H., 2016. Catalytic deoxygenation of bio-oil model compounds over acid-base bifunctional catalysts. *ACS Catal.* 6 (4), 2608–2621. <https://doi.org/10.1021/acscatal.6b00245>.
- Zhou, C., Rosén, C., Engvall, K., 2017. Selection of dolomite bed material for pressurized biomass gasification in BFB. *Fuel Process. Technol.* 167, 511–523. <https://doi.org/10.1016/j.fuproc.2016.11.017>.